Phosphorylation influences water and ion channel function of AtPIP2;1

Jiaen Qiu[1], Samantha McGaughey[2], Michael Groszmann[2], Steve Tyerman[1], and Caitlin Byrt[2]

[1]University of Adelaide
[2]Australian National University

May 22, 2020

Abstract

The phosphorylation states of two serine residues within the C-terminal domain of AtPIP2;1 (S280, S283) regulate its trafficking to the plasma membrane in response to salt and osmotic stress. Here we investigated whether the phosphorylation states of S280 and S283 also influence AtPIP2;1 facilitated water and cation transport. A series of single and double S280 and S283 phospho-mimic and -deficient AtPIP2;1 mutants were tested in heterologous systems. In Xenopus laevis oocytes, phospho-mimic mutants AtPIP2;1 S280D, S283D and S280D/S283D, had significantly greater ion conductance for Na+ and K+, whereas the S280A single and S280A/S283A double mutants, had greater water permeability. A phospho-mimic-dependent inverse relationship between AtPIP2;1 water and ion transport with a 10-fold change in both was observed. These results revealed that phosphorylation of S280 and S283 influences the preferential facilitation between ion and water permeability by AtPIP2;1. The results also hint at other sites playing a role that are yet to be elucidated. Expression of the phospho-mimic AtPIP2;1 mutants in Saccharomyces cerevisiae, confirmed that phosphorylation influences plasma membrane localisation, and revealed higher Na+ accumulation for S280A and S283D. Collectively, the results show that phosphorylation in the C-terminal domain of AtPIP2;1 influences its subcellular localisation and cation transport capacity.

Introduction

Aquaporins are membrane bound channel proteins that facilitate the passive bidirectional movement of water and other small molecules across biological membranes. Substrates currently known to be transported by aquaporins include gases (O_2; Zwiazek *et al.,*2017, CO_2; Rodrigues *et al.,* 2017; Uehlein*et al.,* 2003), metalloids (silicon; Ma *et al.,* 2006, boron; Takano *et al.,* 2006, arsenic; Li *et al.,* 2009), reactive oxygen species (H_2O_2; Bienert*et al.,* 2007; Dynowski *et al.,* 2008; Hooijmaijers *et al.,* 2012), monovalent cations (Na^+; Byrt *et al.,* 2017; Kourghi *et al.,* 2017; Weaver *et al.,* 1994) and other neutral substrates (urea; Dynowski *et al.,* 2008b, glycerol; Gerbeau *et al.,* 1999, ammonia; Loqué *et al.,* 2005). As facilitators of transmembrane water transport, members of the Plasma membrane Intrinsic Protein (PIP) sub-family have roles in mediating water uptake at the root-soil interface, in transcellular water flow, and in regulating hydraulic conductivity in response to abiotic stresses (for recent reviews see: Chaumont & Tyerman, 2014; Maurel *et al.,* 2015; Gambetta *et al.,* 2017). Similar to some mammalian aquaporin isoforms, a subset of plant PIPs (Arabidopsis PIP2;1 and PIP2;2) were recently found to facilitate the transport of monovalent cations such as Na^+, more evident at low external calcium and high pH (Byrt *et al.,* 2017; Kourghi *et al.,*2017). The ability of some plant aquaporins to facilitate Na^+ transport has implications in relation to plant salinity stress responses and tolerance to osmotic stress (McGaughey*et al* ., 2018).

PIPs are implicated in mediating water uptake from soil to roots and changes to root hydraulic conductivity in response to stress (Tournaire-Roux *et al.,* 2002). In Arabidopsis, root hydraulic conductance correlated

positively with both protein abundance of PIP2 aquaporins and the abundance of phosphorylated PIP2 proteins (di Pietro*et al.,* 2013). Exogenous treatment of barley plants with the kinase inhibitor staurosporine significantly reduced root hydraulic conductance (Horie *et al.,* 2011). The phosphorylation state of several conserved serine residues in the cytoplasmic regions of PIPs, including those in the CTD, have been implicated in a mechanism where phospho-regulation can directly influence water permeation through the pore (Table 1; Johansson *et al.,* 1998; Törnroth-Horsefield*et al.,* 2006; Nyblom *et al.,* 2009; Yaneff *et al.,*2016) and have been demonstrated to change in response to salt or osmotic stress, influencing PIP trafficking and localisation (Boursiac*et al.,* 2005; Boursiac *et al.,* 2008; Li *et al.,*2011; Prak *et al.,* 2008). The phosphorylation state of two serine residues on the CTD of AtPIP2;1, S280 and S283, has been reported to change in plant roots exposed to salt treatments and the phosphorylation of S283 has been associated with the salt-induced internalisation of AtPIP2;1 in Arabidopsis roots (Prak *et al.,* 2008).

Extensive studies on aquaporin regulation in animals has also identified phosphorylation as a key regulator of animal aquaporin channel function (both water and ion), protein cycling, trafficking, and membrane localisation (Table 1). The water and ion channel function of soybean (*Glycine max*) NOD-26 (GmNOD-26), the first plant aquaporin to be identified as permeable to both water and ions, was shown to be regulated by the phosphorylation of a CTD residue S262 (Guenther*et al.,* 2003; Lee *et al.,* 1995; Weaver *et al.,*1994). Phosphorylation of S262 altered the voltage sensitivity of GmNOD-26 ion channel activity (Lee *et al.,* 1995) and increased its osmotic water permeability (Guenther *et al.,* 2003). GmNOD-26 phosphorylation was also reported to increase in plants exposed to osmotic stress (Guenther *et al.,* 2003). It is therefore conceivable that phosphorylation could augment the ability of PIPs to facilitate water and Na^+ transport in isoforms capable of such activity. In which case, changes in phosphorylation states would not only regulate PIP protein trafficking and localisation in response to salt and osmotic stresses but also water and Na^+transport capacity (Byrt *et al.,* 2017; McGaughey *et al.,*2018).

In this study the phosphorylation state of the two conserved CTD serine residues (S280 and S283) in AtPIP2;1 was investigated through series of single and double S280 and S283 phospho-mimic and -deficient AtPIP2;1 mutants in the context of the concurrent regulation of ion (Na^+ and K^+) and water transport. It is important to determine the relationships between PIP protein regulation by phosphorylation and water and ion transport capacity because these features influence plant tolerance to drought and NaCl stresses (McGaughey *et al* ., 2018). Our results indicate that phosphorylation has a key role to play in AtPIP2;1 regulation of transport selectivity and capacity. Given existing information about the regulation of animal aquaporins, and how precisely channel activity, trafficking and localisation are co-ordinately controlled (Table 1), it is expected that there is similar complexity in the regulation of plant aquaporin function that are yet to be fully explored.

Table 1: Examples of regulation of aquaporins by phosphorylation.

AQP isoform	P site	P state (+/-)	Influence on protein	Influence on protein	Influence on protein	Influence on protein	Experimental methods	Experimental methods	Expression system
			W	**I**	T	L	SDM	Pharm.	
AQP2	Ser-256	+	—						PL, KC, LLC
	Ser-269	+							KC
	Ser-264	+							IN (rat, mouse)
AQP4	Ser-180	+	—						LLC
	Ser-111	+	—						AC
AQP1	Thr-157	+	—	—					O

AQP isoform	P site	P state (+/-)	Influence on protein	Influence on protein	Influence on protein	Influence on protein	Experimental methods	Experimental methods	Expression system
	Thr-239	+	—	—					
	Tyr-253	+		—					O
BIB	Tyr-?	+		—					O
PpAQY1	Ser-107	+	—						SP
α-TIP	Ser-7	-	—						O
	Ser-23	-	—						
	Ser-99	-	—						
AtPIP2;1	Ser-121	+	—						O, PP
	Ser-280	+	?						IP (transgenics), PP
	Ser-283	+	?						
GmNOD26	Ser-262	+		—					PLB
	Ser-262	+	—						O
SoPIP2;1 (PM28A)	Ser-115	+	—						O
	Ser-274	+	—						
ZmPIP2;1	Ser-126	-	—						O
	Ser-203	-	—						
	Ser-285	+/-	NE						
CsPIP2;1	Ser-121	-	—						O
	Ser-273	-	—						

P: phosphorylation, P state +/-: phosphorylated or phospho-mimic and dephosphorylated or phospho-deficient respectively, W: water conductance, I: ion conductance, T: trafficking and/or protein cycling, L: protein localisation, SDM: phosphorylation or dephosphorylation mimic by site-directed mutagenesis, Pharm.: phosphorylation changes by application of pharmacological agents (kinase inhibitors or kinase activators). A — or — in the water or ion conductance column indicates if there was an increase or decreased observed; NE: No effect on function reported. In the expression systems column, O: *Xenopus laevis* oocytes; PL: proteoliposomes; PLB: planar lipid bilayers; KC: kidney cells; LLC: LLC-PK1 cells; AC: astrocyte cells; SP: spheroplasts; PP: protoplasts; IN: *in vivo* , IP: *in planta* . A blank box indicates it has not been reported on/tested.[1] Eto *et al.,* 2010;[2] Lu *et al.,* 2008;[3] Moeller *et al.,* 2010;[4] Van Balkom *et al.,* 2002;[5] Hoffert *et al.,* 2006;[6] Hoffert *et al.,* 2008;[7] Moeller *et al.,* 2010[8] Fenton *et al.,* 2008;[9] Zelenina *et al.,* 2002;[10] Gunnarson *et al.,* 2005;[11] Zhang *et al.,* 2007;[12] Campbell *et al.,* 2012;[13] Yanochko and Yool, 2002;[14] Fischer *et al.,* 2009;[15] Maurel *et al.,* 1995;[16] Grondin *et al.,* 2015;[17] Prado and Maurel, 2013;[18] Prak *et al.,* 2008;[19] Qing *et al.,* 2016;[20] Lee *et al.,* 1995;[21] Weaver *et al.,* 1994;[22] Guenther *et al.,* 2003;[23] Johansson *et al.,* 1998;[24] Van Wilder *et al.,* 2008;[25] Jang *et al.,* 2014.

Materials and methods

Cloning, preparation of oocyte constructs and cRNA synthesis

The AtPIP2;1 (At3g53420) coding sequence was cloned using high-fidelity Phusion® polymerase (New England Biolabs, USA) from Arabidopsis root cDNA into a Gateway-enabled pCR8/GW/TOPO entry vector (Life Technologies) before being transferred into the pGEMHE (DEST) vector using LR clonase II (Invitrogen). Primers were designed to generate site-directed single and double point phosphomimetic

mutations in AtPIP2;1 (Table S1) using AtPIP2;1 in pGEMHE as a template. All the constructs in pGEMHE were linearized using restriction enzyme NheI-HF (New England Biolabs, USA) before cRNA was synthesized using mMESSAGE mMACHINE® T7 Transcription kit (Thermo Fisher Scientific, Australia) as previously described Qiu *et al.,* (2016). The concentration and quality of cRNA was determined by NanoDrop and gel electrophoresis.

Preparation of Xenopus laevis oocytes

X. laevis oocytes were harvested and stored following Byrt*et al.,* (2017). Oocytes were injected with 46 nL of RNAse-free water using a micro-injector (Nanoinject II, automatic nanolitre injector, Drummond Scientific) with either no cRNA or 23 ng cRNA. Post injection and prior to experiments oocytes were stored at 18 °C in a Low Na^+ Ringer's solution (62 mM NaCl, 36 mM KCl, 5 mM $MgCl_2$, 0.6 mM $CaCl_2$, 5 mM Hepes, 5% (v/v) horse serum and antibiotics (0.05mg mL^{-1}tetracycline, 100 units mL^{-1} penicillin/0.1 mg mL^{-1} streptomycin)), pH 7.6 for 24-36 h. Expression of AtPIP2;1 within each oocyte batch was confirmed via burst test following Byrt *et al.,* (2017).

Oocyte water permeability

Osmotic water permeability (P_{os}) of oocytes injected with water or cRNA was determined following Byrt *et al.,* (2017) with the following important exception based on the previous finding of rapid Na^+ efflux when the external Na^+ concentration is reduced related to PIP2;1 expression (Byrt *et al.,* 2017): oocytes were pre-incubated in 3 mL iso-osmotic solution (5 mM NaCl, 2 mM KCl, 1 mM $MgCl_2$, 50 μM $CaCl_2$, pH 8.5) with an osmolality of 240 mosmol.kg^{-1} (adjusted with D-mannitol) for 1 h prior to being transferred to a solution with the same ionic composition (5 mM NaCl, 2 mM KCl, 1 mM $MgCl_2$, 50 μM $CaCl_2$, pH 8.5) with an osmolality of 45 mosmol.kg^{-1} for the photometric swelling assay.

Electrophysiology

Two-electrode voltage clamp (TEVC) recordings were performed on *X. laevis* oocytes 24-36 h post injection. Preparation of glass pipettes was as described in Byrt *et al.,* (2017). TEVC experiments were performed using an Oocyte Clamp OC-725C (Warner Instruments, Hamden, CT, USA) with a Digidata 1440A data acquisition system interface (Axon Instruments, Foster City, CA, USA). Injected oocytes were continuously perfused with solution after being pierced with the voltage and current electrodes and allowed to stabilise. TEVC was performed in solutions consisting of 50 mM NaCl (Na50), 100 mM NaCl ('Na100') or 100 mM KCl ('K100') in a basal solution (2 mM KCl, 1 mM $MgCl_2$ and 5 mM HEPES, osmolality was adjusted to 240 mosmol.$kg^{-1}$with D-mannitol) with 50 μM $CaCl_2$ and pH 8.5. For experiments involving endogenous oocyte kinase stimulation or inhibition, injected oocytes were incubated prior to TEVC in Low Na^+ Ringers (described previously) supplemented with 1 mM 8-Br-cAMP (Sigma (St Louis, MO, USA), #B5386), or 1 mM 8-Br-cGMP (Sigma, #B1381) or 10 μM H7 dihydrochloride (Sigma, #17016) from concentrated stocks dissolved in water. Steady–state currents were recorded starting from –40 mV holding potential for 0.5 s and ranging from 40 mV to –120 mV with 20 mV decrements for 0.5 s before following a –40 mV pulse for another 0.5 s. Ionic conductance was calculated by taking the slope of a regression of the linear region across the reversal potential (–60 mV to +40 mV). TEVC recordings were analysed with CLAMPEX 9.0 software (pClamp 9.0 Molecular Devices, CA, USA).

Oocyte Na^+ Content

Water control and cRNA injected oocytes were incubated for 24 h in the 'Na100' solution as was used for electrophysiology recordings. Oocytes were removed to individual 1.5 mL microfuge tubes and washed briefly with double distilled H_2O. All solution was removed from the tube and oocytes were stored at –20°C. Oocytes were thawed at room temperature before being homogenised in 0.1 M analytic nitric acid and digested at 42°C for 2 h. Nitric acid digested homogenates were diluted 1:10 with double distilled H_2O, vortexed briefly and centrifuged at 16 000 x g (Beckman Coulter Microfuge® 16) to pellet cell debris. An aliquot of the supernatant was removed for dilution and ion analysis was performed using an Atomic Absorption Spectrophotometer (AAS; Shimadzu AA-7000) according to manufacturer's instructions.

Yeast vector cloning and yeast localisation

Gateway compatible entry clone containing *AtPIP2;1* was generated in pENTR1a and used as a template to generate site-directed single and double point phosphomimetic mutations in AtPIP2;1 (Table S1). Additional non-stop codon versions of these genes were PCR amplified from the pENTR1a clones with primers containing attB sites and inserted into pZeo using BP clonase (Invitrogen). The pZeo non-stop-codon gene versions were shuttled into pAG426-GPD-eGFP by LR clonase II reaction (Invitrogen) to create C-terminal GFP fusion for sub-cellular protein localisation. The pAG426-GPD-GFP vector which confers strong constitutive transgene expression in yeast, were obtained from Addgene (plasmid #14150) and originally deposited by Susan Lindquist (Alberti*et al.,* 2007). The pAG426-GPD-GFP AtPIP2;1 wild-type and the single and double AtPIP2;1 S280 and S283 phosphorylation mutant constructs were transformed into the Saccharomyces cerevisiae*aqy1/aqy2* double mutant yeast strain (Matα· leu2::hisG; trp1::hisG, his3::hisG; ura352 aqy1D::KanMX aqy2D::KanMX) using Frozen-EZ Yeast Transformation II kit (Zymo Research). The*aqy1/aqy2* double mutant yeast strain was gifted by Peter Dahl (Hohmann Lab) (Tanghe *et al.,* 2002).

Sub-cellular GFP signal was visualised on a Zeiss LSM780 confocal laser-scanning microscope (Carl Zeiss) operated by Zen Black software and a DIC x40 oil immersion lens. eGFP was excited at 488nm and emission was captured at 495-570nm and RFP was excited at 561nm and emission captured at 580-735, with 24 µm pinhole and master and digital gains identically set for all images and analysis. Between 30 to 160 cells for each of the AtPIP2;1 wild-type and mutant proteins were scored across 3-4 independent experiments with differences in the localisation patterns between the genotypes consistent across sessions. pSM1959 was obtained through Addgene (Susan Michaelis - Addgene plasmid #41837; Metzger *et al.,* 2008).

Yeast Na^+ Content

The full-length cDNA of AtPIP2;1 and AtPIP2;1 single- and double-point C-terminal phosphorylation mutations (Table 1) generated in gateway enabled entry vectors were sub-cloned into pYES-DEST 52 (Invitrogen) yeast expression destination vector driven by *GAL1* promoter through LR reaction. Empty vector and AtPIP2;7 (following Kourghi*et al.,* 2018) were also included as negative controls. Confirmed constructs were transformed into *S. cerevisiae* strain B31 (*$\Delta\epsilon\nu a1::HI\Sigma3::\epsilon\nu a4$, $\Delta\nu\eta a1::\Lambda E\Upsilon2$*) (Bañuelos *et al.,* 1998) using Frozen-EZ Yeast Transformation II kit (Zymo Research). Successful transformants grown on selective media (Amino acids supplements drop-out without uracil (Sigma), 0.67 % (W/V) Na^+-free Yeast nitrogen base (Formedium), 10 mM MES, 2% glucose (W/V), 2% agar (W/V) and pH 5.6) were inoculated into same liquid media for overnight incubation at 30 °C with shaking. The overnight yeast cultures were diluted to 0.05 at OD_{600nm} before further growing in liquid media containing 2% galactose (W/V) to induce the gene expression in B31 yeast for 18 h. To test the Na^+influx, yeast culture were first centrifuged at 2,500 x *g* for 3 min and the supernatant was removed. Yeast cells were then gently resuspended in Na^+ uptake buffer (70 mM NaCl, 10 mM MES, 10 mM EGTA, pH 5.6) and incubated at 30 °C for 40 min before being harvested through a 0.45 µm Millipore filter (Merck). Yeast pellets collected by Millipore filter were washed three times using ice-cold washing buffer (20 mM $MgCl_2$ and D-mannitol to adjust the osmolarity similar to Na^+ uptake buffer). To reduce the potential for uncontrolled ion fluxes across yeast membrane during wash, a running vacuum was connected to the Millipore filter to quickly remove the supernatant and washing buffer. Harvested yeast samples were dried on the Millipore filter at 70 °C for two days and were digested in 1% HNO_3 acid at same temperature for another 2 days. Digested yeast sample was vortexed and centrifuged briefly at 13,000 x g and the supernatant was diluted with MilliQ water. Yeast Na^+ and K^+ contents were measured using Atomic Absorption Spectrophotometer (AAS; Shimadzu AA-7000) according to manufacturer's instructions.

Results

Cyclic nucleotide and kinase inhibitor treatments influence AtPIP2;1 mediated ionic conductance in X. laevis oocytes

AtPIP2;1 expression in *X. laevis* oocytes elicits currents in the presence of Na^+ (Byrt *et al.,* 2017). We

investigated whether AtPIP2;1-facilitated ion transport may be altered by its phosphorylation state. The activity of endogenous kinases in*X. laevis* oocytes, and hence phosphorylation state of expressed proteins, were manipulated by the exogenous application of membrane permeable cyclic nucleotide monophosphate (cNMP) analogues 8-Br-cAMP and 8-Br-cGMP as kinase stimulators, and the kinase inhibitor H7 (Figure 1). These pharmacological agents have been used previously in this heterologous system to manipulate kinase activity for testing the functional regulation of mammalian aquaporins by phosphorylation (Campbell *et al.,* 2012; Han and Patil, 2000; Hoffert *et al.,* 2008; Yool *et al.,* 1996).

Oocytes were injected with water or *AtPIP2;1* cRNA and either kept untreated as a control, or incubated in 1 mM 8-Br-cAMP (cAMP) or 8-Br-cGMP (cGMP) for 10 min, or incubated in 10 μM H7 for 2 h, or incubated in H7 prior to a cNMP incubation. The ionic conductance of these oocytes was measured by TEVC (Figure 1). Data was collected from multiple independent oocyte batches; therefore, to remove batch-to-batch variation in native ionic conductance and examine only the response to the treatments the data for treated water injected oocytes were normalised to untreated water injected oocytes (Figure 1a), and treated AtPIP2;1 injected oocytes were normalised to untreated AtPIP2;1 injected oocytes (Figure 1b) within each batch. The representative IV curves of AtPIP2;1 and water injected oocytes are indicated in Figure S1.

Water injected oocytes did not respond to any treatment type, with the exception of a slight increase in conductance that was observed upon cGMP treatment when compared to H_2O injected oocytes treated with cAMP (Figure 1a). Incubation of AtPIP2;1 injected oocytes in solutions containing H7 resulted in a significant decrease in ionic conductance relative to untreated (Figure 1b). In contrast, incubation in cAMP increased the ionic conductance of AtPIP2;1 injected oocytes (Figure 1b). AtPIP2;1 injected oocytes that were first incubated in H7 followed by a cAMP incubation had increased ionic conductance compared to those incubated only in H7. This indicates that Na^+transport facilitated by AtPIP2;1 in oocytes is potentially influenced by phosphorylation status, assuming that the treatments alter endogenous kinase activity that phosphorylate AtPIP2;1. It has previously been demonstrated that *X. laevis* can phosphorylate an expressed PIP2 aquaporin (Johansson *et al.,* 1998).

Phospho-mimic and deficient AtPIP2;1 mutants had altered ionic conductance and Na^+ accumulation in X. laevis oocytes

The phosphorylation state of AtPIP2;1 CTD residues S280 and S283 is altered *in planta* by salt treatments (Prak *et al.,* 2008). To explore the potential regulatory roles of S280 and S283 phosphorylation on AtPIP2;1-facilitated ion transport, single and double S280 and S283 phospho-mimics mutated to aspartic acid (D), or phospho-deficient mutated to alanine (A) versions of AtPIP2;1 were generated. The ionic conductance of oocytes expressing AtPIP2;1 wild-type (WT) or AtPIP2;1 phospho-mimic (S280D, S283D) and phospho-deficient (S280A, S283A) single and double mutants in the presences of Na^+ and K^+ were measured by TEVC (Figure 2, Figure S2).

In the 'Na100' solution the single and double phospho-deficient-mimicking mutants S280A, S283A and A/A induced currents and had ionic conductance of similar magnitude to that of AtPIP2;1 WT (Figure 2a-d). Whereas, the expression of the single phosphorylation-mimicking mutants S280D and S283D and the double phosphorylation-mimicking mutants D/A, A/D and D/D induced greater currents and ionic conductance than WT or the phospho-deficient mutants (Figure 2a-d).

AtPIP2;1 WT was also able to elicit somewhat larger currents and conductances (20-30% larger) with K^+ as the major univalent cation (Figure 2a,c). The phosphorylation mutants had similar effects on conductance in a 'K100' solution to that observed in the 'Na100' solution. The phospho-mimics S280D and S283D had greater ionic conductance than either AtPIP2;1 WT or the phospho-deficient mutants (Figure 2c).

The total Na^+ content of AtPIP2;1 WT and phospho-mutant expressing oocytes after 24 h incubation in 'Na100' solution was determined by analysis with an atomic absorption spectrophotometer (Figure 2e). Consistent with the trends observed for ionic conductance in the same solution ('Na100'; Figure 2c,d), the phospho-mimic single (S280D and S283D) and double mutants (A/D, D/A, D/D) accumulated greater Na^+

per oocyte than WT (Figure 2e). The phospho-deficient mutants (S280A, A/A) accumulated similar Na^+ to AtPIP2;1 WT oocytes with the exception of S283A, which had significantly higher Na^+accumulation and an opposite trend to that observed for ionic conductance (Figure 2a,c,e).

Relationship between phosphorylation, water permeability and ionic conductance of AtPIP2;1

Mutant versions of AtPIP2;1 where different phosphorylation states for CTD sites S280 and S283 were mimicked differed in their osmotic water permeability (P_{os}) and ionic conductance when expressed in oocytes (Figure 2, Figure S2, Figure 3, Figure S3 and Figure S4). For each individual oocyte included in the experiment measurements of both P_{os} and ionic conductance were captured so that the relationship between P_{os} and ionic conductance could be investigated.

The P_{os} of oocytes expressing AtPIP2;1 WT, and AtPIP2;1 S280 and S283 single and double phospho-mimic and -deficient mutants was determined via the photometric swelling assay (Figure S4). The single and double phospho-deficient mutants A/A had greater mean P_{os} relative to AtPIP2;1 WT (Figure S4). Comparatively, the single and double phospho-mimic mutants S280D, S283D, D/A, A/D and D/D all had lower mean P_{os} compared to AtPIP2;1 WT (Figure S4). The lower P_{os} for the D/A and A/D mutants indicates that when either of the S280 or S283 sites are phosphorylated this is likely having a dominant functional effect over the dephosphorylated state of the other site. It was also evident that the variation between individual oocytes in both P_{os} and ion conductance was dependent on the mutation (Figure 2 c, d & Figure S4)

To test for a relationship between P_{os}, ionic conductance and CTD phosphorylation state, TEVC was first performed followed by swelling assays on the same oocytes after a 2 h recovery incubation. Data was collected from multiple independent oocyte batches. Individual conductance was plotted against the corresponding P_{os} for each oocyte (Figure S3). For WT and D/D the variation in both ionic conductance and P_{os} showed a clear and significant inverse correlation (Figure S3). A significant inverse linear regression was also observed when all genotypes were combined (Figure S3). To better illustrate the relationship, all data points were binned on the basis of ionic conductance (10 μS bins) regardless of genotype (Figure 3a. The negative correlation between P_{os} and ionic conductance was best fit to a single exponential decay ($p < 0.005$) (Figure 3a) such that a high ionic conductance corresponded to a lower P_{os} similar in level to that of water injected controls (dashed horizontal blue line in Figure 3b). This indicates that phosphorylation at AtPIP2;1 CTD affects the ion/water permeability in a reciprocal but variable manner, whereby at the maximum ionic conductance the P_{os} of PIP2;1 is effectively zero, and when P_{os} was maximal the ionic conductance of PIP2;1 expressing oocytes effectively reduced to zero (i.e. similar to water injected control oocytes; dashed vertical red line Figure 3a and c).

To illustrate the trend with the different CTD mimics the frequency distributions are shown for decreasing P_{os} (Figure 3b) and increasing ion conductance (Figure 3c) The red (vertical) and blue (horizontal) dashed lines indicate the means of ionic conductance and P_{os} respectively for H_2O injected oocytes (Figure 3a, b, c). AtPIP2;1 A/A, S283A, A/D and S280D mutants follow the same relative order for the change in mean P_{os} and ionic conductance (Figure 3d).

The AtPIP2;1 single and double phosphorylation mutants with at least one phospho-mimic residue (S280D, S283D, A/D, D/A, D/D) had greater mean ionic conductance and reduced mean P_{os} relative to AtPIP2;1 WT (Figure 3b, c). The S280D, S283D and D/D mutants exhibited increased frequency of a clustered population with significantly down-regulated P_{os}, in contrast to AtPIP2;1 WT and other mutants that showed a wide distribution of P_{os} (Figure 3b). The different distribution patterns observed in ionic conductance and P_{os} for the S280 and S283 phosphorylation mimics suggests that other factors or phosphorylation states may be altered in oocytes to cause variation.

Phospho-mimic and deficient AtPIP2;1 mutants had altered Na^+ accumulation in S. cerevisiae strain B31

To test whether mimicking AtPIP2;1 C-terminal phosphorylation states influenced cell Na^+ accumulation in yeast, the phospho-mimic and deficient mutants were expressed in a Na^+ efflux compromised strain B31 (*Δενα1::ΗΙΣ3::ενα4, Δνηα1::ΛΕΥ2*). This strain is deficient in Na^+ efflux (Bañuelos *et al.,* 1998) enab-

ling greater potential to distinguish any differences in intracellular Na^+ accumulation under salt treatment associated with Na^+ uptake through plasma membrane localised Na^+ transporters. Na^+ accumulation in B31 yeast expressing phospho-mimic and deficient AtPIP2;1 mutants was measured after the yeast had been incubated in a 70 mM NaCl uptake buffer for 40 min. The yeast cell Na^+ accumulation was measured in samples representing all controls and mutants before and after the uptake assay and no significant differences in yeast cell sodium content were observed in the samples prior to the incubation in the NaCl uptake buffer (Figure S5a).

Yeast expressing AtPIP2;1 WT accumulated greater Na^+than the empty vector control and AtPIP2;7 (Figure 4). AtPIP2;7 was used as an additional control as this PIP was previously reported to lack Na^+ induced currents when expressed in *X. laevis* oocytes (Kourghi *et al.,* 2017). Comparison of Na^+ accumulation for yeast expressing each of the single and double phospho-mimic/deficient mutants of interest, showed that only yeast expressing AtPIP2;1 S280A and S283D accumulated significantly more Na^+ than the empty vector controls (Figure 4). However, mimicking single phosphorylation and de-phosphorylation mutations at S280 and S283 sites influenced Na^+ accumulation (Figure 4). Yeast expressing AtPIP2;1 S280A accumulated significantly greater Na^+ than S280D. Whereas greater Na^+ accumulation was observed for S283D relative to S283A (Figure 4). In the case of A/D and D/A, although yeast expressing both double mutants had Na^+contents not significantly different to the empty vector control, A/D caused significantly greater Na^+ accumulation than D/A (Figure 4). Interestingly, when both CTD sites were mimicked in either a phosphorylated or de-phosphorylated state, (D/D and A/A), a similar level of Na^+ accumulation was observed not significantly different to that of empty vector controls (Figure 4).

AtPIP2;1 WT and CTD mutants were capable of facilitating K^+ transport in *X. laevis* oocytes (Figure 2A and C). To examine whether similar trends occur when the proteins of interest were expressed in yeast, the K^+ contents of yeast samples were examined. Prior to the incubation in the NaCl uptake buffer there were no significant differences observed between genotypes (Figure S5b). This was also the case after incubation in the 70 mM NaCl buffer solution for 40 min (Figure S6).

Phosphorylation state of S280 and S283 influences AtPIP2;1 localisation in yeast

Mimicking changes in C-terminal phosphorylation states of AtPIP2;1 not only altered Na^+ and H_2O conductance in *X. laevis* oocytes (Figure 2 and 3), but also influenced the sub-cellular localisation of AtPIP2;1 in *S.cerevisiaeaqy1/aqy2* double mutant yeast strain (Figure 5). Sub-cellular localisation tendencies of the *AtPIP2;1* phospho-mutants were monitored in yeast using both N- or C-terminal GFP fusions. Fusion of AtPIP2;1 wild-type or AtPIP2;1 phospho-mutants to GFP, redirected GFP from a diffuse cytosolic pattern (Figure 5A) to a predominantly sharp ring around the cell perimeter coinciding with the plasma membrane (PM; Figure 5C-I). Weaker GFP signal associated with the tonoplast of the vacuole was also frequently observed. In addition, a proportion of cells showed internal and patchy perimeter GFP signal, matching the localisation pattern of the SEC63::RFP endoplasmic reticulum (ER) marker (Figure 5B). The detectable frequency and intensity of the ER co-localisation differed between the AtPIP2;1 wild-type and some of the AtPIP2;1 280/283 phospho-mimic mutants (Figure 5J). A difference was observed for the AtPIP2;1 S280D mutant, which had frequently occurring intense GFP signal co-localising to the ER (Figure 5D, E and J), relative to the trend observed for the AtPIP2;1 S283D and AtPIP2;1 D/D mutants, which had distinct GFP signal around the perimeter consistent with PM localisation, and less frequent or intense ER co-localisation (Figure 5F, G, H and J). The tendency of the AtPIP2;1 S280A and A/D mutants to co-localise to the ER was more likely than for wild-type (Figure 5I and J). GFP localisation patterns for the phospho-deficient AtPIP2;1 S283A and A/A mutants along with the D/A mutant were equivalent to that of wild-type AtPIP2;1 (Figure 5J). There was no discernible difference in the localisation patterning whether the GFP was fused to the N- or C- terminal (data not shown).

Comparisons between the phospho-mutants reveal co-ordinated effects of positions S280 and S283 in determining sub-cellular localisation. The more prominent PM targeting of the AtPIP2;1 D/D mutant in comparison to the A/A, D/A, or A/D mutants, indicates that mimicking of phosphorylation of both S280 and S283 was required to promote more distinctly PM localisation (Figure 5J). The distinct ER co-localisation of AtPIP2;1

S280D was not observed in either of the two other S280D phospho-mimic mutants (D/A or D/D) (Figure 5J), indicating that a serine at position 283 could be specifically required in combination with the phospho-mimic aspartic acid at position 280 to achieve the distinct ER co-localisation.

Discussion

AtPIP2;1 is able to facilitate water and monovalent cation transport activity *in vivo* , and this function is influenced by the phosphorylation states of CTD residues S280 and S283 (Figures 1-4). In*X. laevis* oocytes, S280 and S283 phosphorylation status influenced the transport function of AtPIP2;1, such that relatively greater water transport occurred when these sites mimicked an un-phosphorylated state and greater ion transport occurred when they mimicked a phosphorylated state (Figure 2 and 3). A phosphorylation-dependent inverse relationship was observed for AtPIP2;1-facilitated water transport relative to ion transport (Figure 3 and Figure S3, 4), where there was approximately ten-fold changes in both permeabilities (Figure S3). Yeast expressing the different AtPIP2;1 S280 and S283 mutation combinations accumulated different amounts of intracellular Na^+ following incubation in a buffer containing 70 mM NaCl (Figure 4). S280 and S283 phosphorylation status also influences the distribution and abundance of AtPIP2;1 protein localising between the ER and PM in yeast (Figure 5).

AtPIP2;1 facilitated ion transport is influenced by activity of endogenous oocyte kinases

Stimulation or inhibition of the endogenous kinase activity of *X. laevis* oocytes expressing wild-type (WT) AtPIP2;1 was manipulated by treatment with cyclic nucleotide monophostphates (cNMPs) or a kinase inhibitor (H7). These treatments resulted in changes in the magnitude of AtPIP2;1-associated ionic conductance when compared to untreated AtPIP2;1 or either treated or untreated water injected control oocytes (Figure 1). Treatments with cAMP and cGMP can stimulate oocyte endogenous kinase activity, and this can alter protein phosphorylation (Glass and Krebs, 1980; Kuwahara *et al.,* 1995). Different kinases respond to cAMP verses cGMP signalling, and the kinases responding to these different signals have different target sites (Conti *et al.,* 2012). Endogenous oocyte kinases have been previously shown to alter plant aquaporin phosphorylation state and influence their water channel activity, and this was demonstrated by applying treatments with kinase stimulators and inhibitors (Maurel *et al.,* 1995; Van Wilder *et al.,* 2008). Treatment of AtPIP2;1 expressing oocytes with cAMP or cGMP increased and decreased AtPIP2;1-associated ionic conductance, respectively (Figure 1). Treatment of AtPIP2;1 expressing oocytes with the kinase inhibitor H7 decreased AtPIP2;1-associated ionic conductance (Figure 1b). H7 treatment similarly reduced aquaporin-associated ionic conductance for HsAQP1 expressing oocytes by inhibiting the influence of cAMP on endogenous kinases (Yool *et al.,* 1996). The different responses to the different cNMP treatments indicate that multiple phosphorylation sites, such as candidate sites in the CTD may be involved in regulating AtPIP2;1-facilitated ionic conductance and that transport function can be altered by the activity of endogenous oocyte kinases. However, a direct effect of cNMPs on AtPIP2;1 may also be possible; HsAQP1 ion channel function is activated by direct cGMP binding to its loop D in a phosphorylation-dependent manner (Anthony *et al.,* 2000; Campbell *et al.,* 2012) although an equivalent site is not present in AtPIP2;1.

Phosphorylation status of C-terminal S280 and S283 sites regulate AtPIP2;1 facilitated water and ion transport

The influence of mutating AtPIP2;1 S280 and S283 sites to phospho-mimic and phospho-deficient versions on channel water and ion transport function was tested in oocytes (Figures 2-3, Figure S4). Oocytes expressing the single phospho-mimic versions of AtPIP2;1, S280D and S283D or the phospho-mimic double mutants A/D, D/A and D/D had greater ionic conductance in solutions containing Na^+ and K^+ and increased internal Na^+content compared to oocytes expressing either AtPIP2;1 WT or the single phospho-deficient variants S280A and S283A or the double phospho-deficient mutant A/A (Figure 2). Oocytes expressing the single mutant S280A and double mutant A/A had greater P_{os} than the other versions (Figure S4). When the phosphorylation status of both CTD sites were controlled but only one site mimicked a phosphorylated state the effect of the phospho-mimicked residue presided somewhat over the effect of the phosphor-deficient

site; for example, both the D/A and A/D phospho-mutants had water and ion transport more similar to that of the D/D mutants than the A/A mutants (Figure 2 and 3). Previously the Rattus AQP2 was reported to be phosphorylated at two serines on its CTD in renal epithelial cells in response to vasopressin, and the effect of phosphorylation of one residue presided over the channel function and trafficking (Table 1) (Lu *et al.,* 2008). The phosphorylation of several CTD residues in Rattus AQP2 also exhibit a hierarchy where the phosphorylation of particular residues does not occur unless the phosphorylation of another site has preceded it (Hoffert *et al.,*2008).

AtPIP2;1 facilitated the transport of K^+ and the single phospho-mimic mutants conferred greater K^+associated conductance than the other versions, similar to the trend observed for phospho-mimic versions for Na^+conductance (Figure 2). AtPIP2;1 and AtPIP2;2 have been proposed as molecular candidates for the elusive non-selective cation channel that have been observed *in planta* (Byrt *et al.,* 2017; McGaugheyet *al.,* 2018; Munns *et al.,* 2019; Demidchik and Tester, 2002; Essah *et al.,* 2003; Roberts and Tester, 1997). The observation that AtPIP2;1 can facilitate K^+ transport i*n vivo* adds support to this hypothesis. The NSCCs observed by Demidchik and Tester, (2002), had greater K^+conductance relative to Na^+ conductance (with a selectivity ratio of 1.49:1.00), which is similar to the trend in K^+ relative to Na^+ conductance for AtPIP2;1 when expressed in *X. laevis* oocytes (Figure 2c). The regulation of AtPIP2;1 ion transport by cGMP treatments (Figure 1) is also relevant to previous NSCC observations, because exogenous application of cGMP was previously shown to inhibit NSCCs *in planta* (Essah *et al.,* 2003; Maathuis and Sanders, 2001), and intracellular cGMP concentrations have been reported to increase in response to salinity and osmotic stress treatments (Donaldson *et al.,* 2004; Rubio *et al.,* 2003). Interestingly, a recent review hypothesised that Na^+ influx via AtPIP2;1 may be inhibited by cGMP under salt stress, which is an idea worthy of follow up investigation *in planta* (Isayenkov and Maathuis, 2019). The observation that AtPIP2;1 facilitates transport of the physiologically important element K^+, and the potential for AtPIP2;1 transport of other monovalent ions such as $NH_4{}^+$, indicates that a potential role for PIPs in nutrient acquisition under normal conditions is also worthy of testing *in planta* .

A negative correlation between AtPIP2;1 facilitated water and ion transport was linked to the CTD phosphorylation state (Figure 3a). AtPIP2;1 mutants including S280D, S283D, D/A and D/D, had a greater tendency to facilitate the transport of ions over water compared to that of the phosphorylation deficient mutant A/A (Figure 3b, d). The variance seen for the ionic conductance and P_{os} of the D/D mutant indicates that there are likely to be other additional regulatory sites that were not controlled for in these experiments. Further research is needed to test how many other AtPIP2;1 regulatory sites influence water and ion transport functions and explore whether these sites have any sort of dependence on the status of the CTD sites.

Several General Regulatory Factors (GRFs; also known as 14-3-3 proteins) were recently reported to interact preferentially with AtPIP2;1 when the S280 and S283 sites were phosphorylated, and co-expression of AtPIP2;1 D/D mutant with GRFs 3,4 and 10 in oocytes increased their P_{os} compared to AtPIP2;1 A/A (Prado *et al.,*2019). In the current study it cannot be excluded that AtPIP2;1 could have interacted with an endogenous oocyte GRF protein, or an endogenous aquaporin interacting ion channel. However, the trends observed for AtPIP2;1 CTD status and associated ionic conductance do not appear common to all aquaporins. There are commonalities for CTD phosphorylation trends among some Arabidopsis PIPs, but not all PIPs with these commonalities confer ionic conductance in oocytes. For example, in Arabidopsis AtPIP2;1, AtPIP2;2, AtPIP2;3, AtPIP2;4 and AtPIP2;7 were found to be unphosphorylated, singly phosphorylated at S280 or diphosphorylated at S280 and S283 (Prak *et al.,* 2008), but AtPIP2;7 did not facilitate ion transport when expressed in oocytes (Kourghi *et al.,* 2017) as confirmed here also from a lack of Na^+ uptake into yeast expressing AtPIP2;7. There is also a precedent for plant aquaporins having ion channel functions in the absence of any potential interacting partners, and associations with the CTD status. The soybean (*Glycine max*) Gm-NOD26, produced ion channel activity when reconstituted in lipid bilayers (Weaver *et al.,* 1994). The water and ion channel function of Gm-NOD26 was also found to be regulated by the phosphorylation of a CTD residue S262 (Guenther *et al.,* 2003; Lee *et al.,* 1995).

The exact physiological role of dual water and ion transporting aquaporins in plants remains unknown and may differ in different tissues (McGaughey *et al.,* 2018). When Arabidopsis roots were exposed to a NaCl treatment the phosphorylation states of AtPIP2;1 S280 and S283 residues was observed to change (Prak *et al.,* 2008). Specifically, when plants were treated with 100 mM NaCl the abundance of the S280/S283 disphosphorylated form decreased. Since phosphorylation of S280 and S283 increase AtPIP2;1 ion channel function, this reduction in S280/S283 diphosphorylated AtPIP2;1 may be a mechanism to reduce Na^+ influx (and possibly K^+ efflux) under salt stress. Salt treatment has also been reported to increase AtPIP2;1 location-cycling (Li *et al.,* 2011; Luu *et al.,*2012), and induce AtPIP2;1 internalisation from the plasma-membrane into intra-cellular vesicles in root cells (Boursiac *et al.,* 2005; Prak *et al.,* 2008; Ueda *et al.,* 2016) where internalisation was reported to be dependent on S283 phosphorylation state (Prak *et al.,* 2008). By manipulating the phosphorylation state of the AtPIP2;1 CTD serine residues, we were also able to alter trafficking and abundance of the AtPIP2;1 protein between the PM and ER in yeast (Figure 5). In the yeast system we found that the phospho-mimic S280D mutation resulted in a more consistent localisation of AtPIP2;1 to the ER rather than trafficking to the PM. This feature specifically required the presence of a serine residue at position 283 and could not be replicated by mimicking a phospho-deficient state using alanine. We also observed that consistency in PM targeting was not only dependent on S283 phosphorylation, but also required dual phosphorylation of both S280 and S283, with the presence of a phospho-mimic residue at position 283 potentially influencing the phosphorylation state of S280. Interestingly the localisation of the double phospho-deficient mutant A/A was similar to other phospho-mimic mutants, such as D/A and A/D (Figure 5), where these other mutant versions exhibited much greater ionic conductance than A/A when expressed in *X. laevis* oocytes (Figure 2). This data, alongside the increased P_{os} of A/A relative to the other mutants (Figure 3), indicates that a mis-localisation of the A/A mutant in oocytes is not likely to be the cause of its lower ionic conductance. Furthermore, the fact we could make these observations in yeast using an aquaporin from the distant taxa of plants, indicates the potential for there to have been a shared evolutionary origin for the process of CTD phosphorylation influencing aquaporin trafficking.

The sophisticated relationship between AtPIP2;1 phosphorylation state and AtPIP2;1 trafficking, localisation, and water and ion transport function may be part of a mechanism for rapidly, reversibly and co-ordinately adjusting water and Na^+ or K^+ flux into or out of the cell under salt and osmotic stress.

Phosphorylation states at CTD sites influence AtPIP2;1 facilitated cation transport differently in different heterologous expression systems

In the oocyte system, greater Na^+ and K^+ conductances and intracellular Na^+ accumulation were consistently observed for single and double phospho-mimic mutants relative to the other mutants, regardless of which CTD site was mimicking a phosphorylated state. Oocytes expressing AtPIP2;1 S280D, S283D, D/A, A/D and D/D had significantly greater Na^+ conductance and accumulation. However, the trends for Na^+ accumulation in yeast for the phospho-mimic (S->D) versions were different to that in oocytes. In the B31 yeast system, only the yeast expressing AtPIP2;1 S280A and AtPIP2;1 S283D were observed to have significantly increased net Na^+ accumulation compared to the empty vector control (Figure 4). These results indicate that different S280 and S283 phosphorylation states might have distinct effects on facilitating Na^+ flux through AtPIP2;1 in yeast. Expression of the AtPIP2;1 double phospho-mimic mutant, D/D, in yeast resulted in the accumulation of similar amounts of Na^+ relative to the values for the empty vector control, which differs from the trend in oocytes where there was increased Na^+ accumulation observed for D/D injected oocytes (Figure 2e). The fact that AtPIP2;1 S283D sub-cellular localisation was similar to the D/D mutant (Figure 5J) indicates that S280 maybe endogenously phosphorylated by the yeast for the S/D version, and potentially this could be triggered in response to position 283 being a phospho-mimic residue. It was the D/D version that was also associated with particularly clear PM abundance when expressed in the aqy1/aqy2 mutant yeast. We also observed that AtPIP2;1 WT and phospho-mimic mutants differed in K^+-associated conductance in oocytes (Figure 2), but we did not observe significant differences in K^+ accumulation for these variants when expressed in yeast, following a NaCl treatment (Figure S6). Differences in oocytes relative to yeast cells such as the absence of a vacuole, and associated differences in signalling and regulatory process could result in the different behaviours. Plant aquaporin trafficking to the PM has

been reported to be regulated by syntaxin proteins; for example, it has been shown that AtPIP2;7 trafficking depends on SYP61 (Hachez *et al.,* 2014). Yeast also employs a set of SNAREs to drive a series of membrane fusion events (Burri and Lithgow, 2004), which could also potentially interact with AtPIP2;1 to influence the sub-cellular localization and subsequently affect cation transport capacity. Yeast and oocyte cells have distinct sets of endogenous protein kinases, and there may be other phosphorylation sites within AtPIP2;1 that could be differently phosphorylated in the two systems that control ion conductance. One possibility is that another site may be preferentially phosphorylated in yeast which reduces the ion conductance of the S280D mutant. For this mutant and also the S283D there was a large spread in ion conductances in oocytes ranging from near to that of water injected controls up to the maximum ion conductance observed (Figure 3d) which was not observed in yeast (Figure 4). This could indicate that another site is variably phosphorylated in oocytes that reduces ion conductance while it may be more consistently phosphorylated in yeast.

CTD phosphorylation as part of a mechanism for gating water and ion transport

The central pore, formed in the middle of the four monomeric channels, has been proposed to be the exclusive channel for ion transport through the AtPIP2;1 tetramer (Kourghi *et al.,* 2018), however, whether or not water and ion transport events are mutually exclusive are yet to be determined. Phosphorylation at the CTD of AtPIP2;1 has the potential to almost completely block the water transport function of AtPIP2;1 when compared to H_2O injected oocytes without abolishing ion transport (Figure 3b,c and Figure S4). In contrast, the double CTD phosphorylation-deficient mimic showed a tendency to completely prevent the ion transport function without affecting the P_{os}(Figure 3c). These data indicate that manipulation of phosphorylation at the CTD of AtPIP2;1 might provide a key control point for regulating the water and ion gating and net channel selectivity.

Some plant AQPs have been shown to be permeable to multiple types of molecules and PIP2;1 is a special example. Not only does it play roles in maintaining water homeostasis, but it is also involved in multiple signalling processes (Chaumont and Tyerman, 2014; Maurel *et al.,*2015). AtPIP2;1 showed H_2O_2 transport capacity and has been proposed to act as a signalling intermediate involved in ROS detoxification and guard cell signalling (Bienert and Chaumont, 2014; Dynowski *et al.,* 2008a; Rodrigues *et al.,*2017). Phosphorylation at the CTD of AtPIP2;1 and its effect on ion/water selectivity, indicates a capacity to rapidly switch substrates between H_2O and ions (Na^+ and K^+). This could quickly adjust cytosolic osmotic and electrochemical gradients, potentially in the vicinity of the water channel. The phosphorylation status may also change the distribution of ion-specific and H_2O-specific channels on the plasma membrane. In such a case, the membrane density of functional cation-selective AtPIP2;1 could be small depending on the single channel conductance and channel open probability. Only a relatively small number of cation conducting AtPIP2;1 may be needed to change the membrane potential while water transport can be easily substituted for by other AtPIP2 and AtPIP1 aquaporins. In this context AtPIP2;1 could be acting as a signalling module of ionic changes to downstream targets to respond to stress.

Conclusions

The data presented here reveal the potential for differential AtPIP2;1 CTD phosphorylation to be a key factor in the processes controlling water and ion channel transport functions, in addition to localisation trends. Mimicking a phosphorylated state of AtPIP2;1 S280 and S283 sites resulted in a transport function where the Na^+ and K^+ ion conductance reached a magnitude similar to that observed for other plant ion channels expressed in *X. laevis*oocytes; indicating that phosphorylation-dependent ion flux through AtPIP2;1 could hypothetically be significant *in planta* (McGaugheyet *al.,* 2018). Plant aquaporins capable of facilitating ion transport are key candidates for the elusive non-selective cation channels responsible for a large proportion of Na^+ and K^+ flux across the PM (Demidchik and Tester, 2002; Rubio *et al.,* 2010). Further testing is needed to explore the influence of phosphorylation at S280 and S283 on water and ion transport functions *in planta* , and to resolve whether the observations of AtPIP2;1 potential to switch between ion and water channel modes are applicable. Discovering the steps in the processes regulating the switching between ion and water channel functions, and resolving their relationship with osmotic stress tolerance mechanisms, holds great

potential for generating discoveries that support the engineering of future strategies for improving plant productivity in dry and saline environments.

Acknowledgements

We thank Wendy Sullivan for expert technical assistance, and Apriadi Situmorang for assistance with yeast growth. We thank the Grains Research and Development Corporation (GRDC) for supporting S.M through project number 9174824 and an Australian Bureau of Agricultural and Resource Economics GRDC Science and Innovation Award funding to C.B. This research was supported by the Australian Research Council (ARC) in the form of DP190102725, and Future Fellowship for CB (FT180100476); J.Q. and S.T. were supported through the ARC Centre of Excellence in Plant Energy Biology (CE140100008). MG was funded by the ARC Centre of Excellence for Translational Photosynthesis (CE1401000015). The authors acknowledge the facilities and assistance of Microscopy Australia, Centre for Advanced Microscopy, (CAM), Australian National University.

The authors have no conflict of interest to declare.

Author Contributions

Conceived (CB, ST); planned research (all); cloning for oocyte experiments (JQ); preparation of materials for oocyte experiments (JQ/SM); TEVC (JQ/SM); swelling (SM); oocyte ion content (SM); preparation of yeast materials and cloning (JQ/SM/MG); yeast ion content (JQ); yeast localisation (MG); analysis (all); creation of manuscript draft (SM/JQ/MG); plotting figures and tables for paper (JQ/SM/MG); manuscript revision and editing (all).

References

Alberti, S., Gitler, A. D. and Lindquist, S. (2007). A suite of Gateway® cloning vectors for high-throughput genetic analysis in Saccharomyces cerevisiae. *Yeast* **24** , 913–919.

Anthony, T. L., Brooks, H. L., Boassa, D., Leonov, S., Yanochko, G. M., Regan, J. W. and Yool, A. J. (2000). Cloned human aquaporin-1 Is a cyclic GMP-gated ion channel. *Mol. Pharmacol.* **57** , 576–588.

Banuelos, M. a, Sychrova, H., Bleykasten-Grosshans, C., Souciet, J. and Potier, S. (1998). The Nha1 antiporter of *Saccharomyces cerevisiae* mediates sodium and potassium efflux. *Microbiology***144** , 2749–2758.

Bienert, G. P. and Chaumont, F. (2014). Aquaporin-facilitated transmembrane diffusion of hydrogen peroxide. *Biochim. Biophys. Acta - Gen. Subj.* **1840** , 1596–1604.

Bienert, G. P., Moller, A. L. B., Kristiansen, K. A., Schulz, A., Moller, I. M., Schjoerring, J. K. and Jahn, T. P. (2007). Specific aquaporins facilitate the diffusion of hydrogen peroxide across membranes. *J. Biol. Chem.* **282** , 1183–1192.

Boursiac, Y., Chen, S., Luu, D.-T. T., Sorieul, M., van den Dries, N. and Maurel, C. (2005). Early effects of salinity on water transport in *Arabidopsis* roots. Molecular and cellular features of aquaporin expression. *Plant Physiol.* **139** , 790–805.

Boursiac, Y., Boudet, J., Postaire, O., Luu, D.-T. T., Tournaire-Roux, C. and Maurel, C. (2008). Stimulus-induced downregulation of root water transport involves reactive oxygen species-activated cell signalling and plasma membrane intrinsic protein internalization. *Plant J.* **56** , 207–218.

Burri, L. and Lithgow, T. (2004). A complete set of SNAREs in yeast. *Traffic* **5** , 45–52.

Byrt, C. S., Zhao, M., Kourghi, M., Bose, J., Henderson, S. W., Qiu, J., Gilliham, M., Schultz, C., Schwarz, M., Ramesh, S. A., et al.(2017). Non-selective cation channel activity of aquaporin AtPIP2;1 regulated by $Ca^{2+}$and pH. *Plant Cell Environ.***40** , 802–815.

Campbell, E. M., Birdsell, D. N. and Yool, A. J. (2012). The activity of human aquaporin 1 as a cGMP-gated cation channel is regulated by tyrosine phosphorylation in the carboxyl-terminal domain.*Mol. Pharmacol.* **81** , 97–105.

Chaumont, F. and Tyerman, S. D. (2014). Aquaporins: Highly regulated channels controlling plant water relations. *Plant Physiol.* **164** , 1600–1618.

Conti, M., Hsieh, M., Musa Zamah, A. and Oh, J. S. (2012). Novel signaling mechanisms in the ovary during oocyte maturation and ovulation. *Mol. Cell. Endocrinol.* **356** , 65–73.

Demidchik, V. and Tester, M. (2002). Sodium fluxes through nonselective cation channels in the plasma membrane of protoplasts from Arabidopsis roots. *Plant Physiol.* **128** , 379–387.

di Pietro, M., Vialaret, J., Li, G.-W., Hem, S., Prado, K., Rossignol, M., Maurel, C. and Santoni, V. (2013). Coordinated post-translational responses of aquaporins to abiotic and nutritional stimuli in Arabidopsis roots. *Mol. Cell. Proteomics* **12** , 3886–3897.

Donaldson, L., Ludidi, N., Knight, M. R., Gehring, C. and Denby, K. (2004). Salt and osmotic stress cause rapid increases in*Arabidopsis thaliana* cGMP levels. *FEBS Lett.* **569** , 317–320.

Dynowski, M., Schaaf, G., Loque, D., Moran, O. and Ludewig, U.(2008a). Plant plasma membrane water channels conduct the signalling molecule H_2O_2. *Biochem. J.***414** , 53–61.

Dynowski, M., Mayer, M., Moran, O. and Ludewig, U. (2008b). Molecular determinants of ammonia and urea conductance in plant aquaporin homologs. *Febs Lett.* **582** , 2458–2462.

Essah, P. A., Davenport, R. and Tester, M. (2003). Sodium influx and accumulation in Arabidopsis. *Plant Physiol.***133** , 307–318.

Eto, K., Noda, Y., Horikawa, S., Uchida, S. and Sasaki, S.(2010). Phosphorylation of aquaporin-2 regulates its water permeability.*J. Biol. Chem.* **285** , 40777–40784.

Fenton, R. A., Moeller, H. B., Hoffert, J. D., Yu, M.-J., Nielsen, S. and Knepper, M. A. (2008). Acute regulation of aquaporin-2 phosphorylation at Ser-264 by vasopressin. *Proc. Natl. Acad. Sci. U. S. A.* **105** , 3134–3139.

Fischer, G., Kosinska-Eriksson, U., Aponte-Santamaría, C., Palmgren, M., Geijer, C., Hedfalk, K., Hohmann, S., De Groot, B. L., Neutze, R. and Lindkvist-Petersson, K. (2009). Crystal structure of a yeast aquaporin at 1.15 Å reveals a novel gating mechanism. *PLoS Biol.* **7** ,.

Gambetta, G. A., Knipfer, T., Fricke, W. and McElrone, A. J.(2017). Aquaporins and root water uptake. In *Plant Aquaporins* , pp. 133–153. Springer.

Gerbeau, P., Guclu, J., Ripoche, P. and Maurel, C. (1999). Aquaporin Nt-TIP$α$ can account for the high permeability of tobacco cell vacuolar membrane to small neutral solutes. *Plant J.***18** , 577–587.

Glass, D. B. and Krebs, E. G. (1980). Protein phosphorylation catalyzed by cyclic AMP-dependent and cyclic GMP-dependent protein kinases. *Annu. Rev. Pharmacol. Toxicol.* **20** , 363–388.

Grondin, A., Rodrigues, O., Verdoucq, L., Merlot, S., Leonhardt, N. and Maurel, C. (2015). Aquaporins contribute to ABA-triggered stomatal closure through OST1-mediated phosphorylation. *Plant Cell* **27** , 1945–1954.

Guenther, J. F., Chanmanivone, N., Galetovic, M. P., Wallace, I. S., Cobb, J. A. and Roberts, D. M. (2003). Phosphorylation of soybean nodulin 26 on serine 262 enhances water permeability and is regulated developmentally and by osmotic signals. *Plant Cell* **15** , 981–991.

Gunnarson, E., Axehult, G., Baturina, G., Zelenin, S., Zelenina, M. and Aperia, A. (2005). Lead induces increased water permeability in astrocytes expressing aquaporin 4. *Neuroscience* **136** , 105–114.

Hachez, C., Laloux, T., Reinhardt, H., Cavez, D., Degand, H., Grefen, C., De Rycke, R., Inze, D., Blatt, M. R., Russinova, E., et al.(2014). Arabidopsis SNAREs SYP61 and SYP121 Coordinate the Trafficking of Plasma Membrane Aquaporin PIP2;7 to Modulate the Cell Membrane Water Permeability. *Plant Cell* **26** , 3132–3147.

Han, Z. and Patil, R. V (2000). Protein kinase A-dependent phosphorylation of aquaporin-1. *Biochem. Biophys. Res. Commun.***273** , 328–332.

Hoffert, J. D., Pisitkun, T., Wang, G., Shen, R.-F. and Knepper, M. A. (2006). Quantitative phosphoproteomics of vasopressin-sensitive renal cells: Regulation of aquaporin-2 phosphorylation at two sites.*Proc. Natl. Acad. Sci.* **103** , 7159–7164.

Hoffert, J. D., Fenton, R. A., Moeller, H. B., Simons, B., Tchapyjnikov, D., McDill, B. W., Yu, M. J., Pisitkun, T., Chen, F. and Knepper, M. A. (2008). Vasopressin-stimulated increase in phosphorylation at Ser269 potentiates plasma membrane retention of aquaporin-2. *J. Biol. Chem.* **283** , 24617–24627.

Hooijmaijers, C., Rhee, J. Y., Kwak, K. J., Chung, G. C., Horie, T., Katsuhara, M. and Kang, H. (2012). Hydrogen peroxide permeability of plasma membrane aquaporins of *Arabidopsis thaliana* . *J. Plant Res.* **125** , 147–153.

Horie, T., Kaneko, T., Sugimoto, G., Sasano, S., Panda, S. K., Shibasaka, M. and Katsuhara, M. (2011). Mechanisms of water transport mediated by PIP aquaporins and their regulation via phosphorylation events under salinity stress in Barley roots. *Plant Cell Physiol.***52** , 663–675.

Isayenkov, S. V and Maathuis, F. J. M. (2019). Plant salinity stress: Many unanswered questions remain. *Front. Plant Sci.***10** ,.

Jang, H. Y., Rhee, J., Carlson, J. E. and Ahn, S. J. (2014). The Camelina aquaporin CsPIP2;1 is regulated by phosphorylation at Ser273, but not at Ser277, of the C-terminus and is involved in salt- and drought-stress responses. *J. Plant Physiol.* **171** , 1401–1412.

Johansson, I., Karlsson, M., Shukla, V. K., Chrispeels, M. J., Larsson, C. and Kjellbom, P. (1998). Water transport activity of the plasma membrane aquaporin PM28A is regulated by phosphorylation.*Plant Cell* **10** , 451–459.

Kourghi, M., Nourmohammadi, S., Pei, J., Qiu, J., McGaughey, S., Tyerman, S., Byrt, C. and Yool, A. (2017). Divalent cations regulate the ion conductance properties of diverse classes of aquaporins.*Int. J. Mol. Sci.* **18** ,.

Kourghi, M., Pei, J. V, De Ieso, M. L., Nourmohammadi, S., Chow, P. H. and Yool, A. J. (2018). Fundamental structural and functional properties of Aquaporin ion channels found across the kingdoms of life.*Clin. Exp. Pharmacol. Physiol.* **45** , 401–409.

Kuwahara, M., Fushimi, K., Terada, Y., Liqun, B., Marumo, F. and Sasaki, S. (1995). cAMP-dependent Phosphorylation Stimulates Water Permeability of Aquaporin-collecting Duct Water Channel Protein Expressed in Xenopus Oocytes. *J. Biol. Chem.* **270** , 10384–10387.

Lee, J. W., Zhang, Y., Weaver, C. D., Shomer, N. H., Louis, C. F. and Roberts, D. M. (1995). Phosphorylation of Nodulin 26 on Serine 262 affects its voltage-sensitive channel activity in planar lipid bilayers. *J. Biol. Chem.* **270** , 27051–27057.

Li, R. Y., Ago, Y., Liu, W. J., Mitani, N., Feldmann, J., McGrath, S. P., Ma, J. F. and Zhao, F. J. (2009). The rice aquaporin Lsi1 mediates uptake of methylated arsenic species. *Plant Physiol.* **150** , 2071–2080.

Li, X., Wang, X., Yang, Y., Li, R., He, Q., Fang, X., Luu, D.-T., Maurel, C. and Lin, J. (2011). Single-molecule analysis of PIP2;1 dynamics and partitioning reveals multiple modes of*Arabidopsis* plasma

membrane aquaporin regulation. *Plant Cell* **23** , 3780–3797.

Loqué, D., Ludewig, U., Yuan, L. and von Wirén, N. (2005). Tonoplast intrinsic proteins AtTIP2;1 and AtTIP2;3 facilitate NH3 transport into the vacuole. *Plant Physiol.* **137** , 671–680.

Lu, H. J., Matsuzaki, T., Bouley, R., Hasler, U., Qin, Q. H. and Brown, D. (2008). The phosphorylation state of serine 256 is dominant over that of serine 261 in the regulation of AQP2 trafficking in renal epithelial cells. *Am J Physiol Ren. Physiol* **295** , F290–4.

Luu, D. T., Martiniãre, A., Sorieul, M., Runions, J., Maurel, C., Martiniere, A., Sorieul, M., Runions, J. and Maurel, C. (2012). Fluorescence recovery after photobleaching reveals high cycling dynamics of plasma membrane aquaporins in Arabidopsis roots under salt stress.*Plant J.* **69** , 894–905.

Ma, J. F., Tamai, K., Yamaji, N., Mitani, N., Konishi, S., Katsuhara, M., Ishiguro, M., Murata, Y. and Yano, M. (2006). A silicon transporter in rice. *Nature* **440** , 688–691.

Maathuis, F. J. and Sanders, D. (2001). Sodium uptake in*Arabidopsis* roots is regulated by cyclic nucleotides. *Plant Physiol.* **127** , 1617–25.

Maurel, C., Kado, R. T., Guern, J. and Chrispeels, M. J.(1995). Phosphorylation Regulates the Water Channel Activity of the Seed-Specific Aquaporin Alpha-Tip. *Embo J.* **14** , 3028–3035.

Maurel, C., Boursiac, Y., Luu, D. T. D.-T. T., Santoni, V., Shahzad, Z. and Verdoucq, L. (2015). Aquaporins in plants.*Physiol. Rev.* **95** , 1321–1358.

McGaughey, S. A., Qiu, J., Tyerman, S. D. and Byrt, C. S.(2018). Regulating root Aauaporin function in response to changes in salinity. *Annu. Plant Rev.* **1** , 1–36.

Metzger, M. B., Maurer, M. J., Dancy, B. M. and Michaelis, S.(2008). Degradation of a cytosolic protein requires endoplasmic reticulum-associated degradation machinery. *J. Biol. Chem.***283** , 32302–32316.

Moeller, H. B., Praetorius, J., Rutzler, M. R. and Fenton, R. A. (2010). Phosphorylation of aquaporin-2 regulates its endocytosis and protein-protein interactions. *Proc. Natl. Acad. Sci.***107** , 424–429.

Munns, R., Day, D. A., Fricke, W., Watt, M., Arsova, B., Barkla, B. J., Bose, J., Byrt, C. S., Chen, Z., Foster, K. J., et al. (2019). Energy costs of salt tolerance in crop plants. *New Phytol.*

Nyblom, M., Frick, A., Wang, Y., Ekvall, M., Hallgren, K., Hedfalk, K., Neutze, R., Tajkhorshid, E. and Törnroth-Horsefield, S.(2009). Structural and functional analysis of SoPIP2;1 mutants adds insight into plant aquaporin gating. *J. Mol. Biol.* **387** , 653–668.

Prado, K. and Maurel, C. (2013). Regulation of leaf hydraulics: from molecular to whole plant levels. *Front. Plant Sci.***4** ,.

Prado, K., Cotelle, V., Li, G., Bellati, J., Tang, N., Tournaire-Roux, C., Martiniere, A., Santoni, V., Maurel, C., Martiniere, A., et al. (2019). Oscillating aquaporin phosphorylations and 14-3-3 proteins mediate circadian regulation of leaf hydraulics. *Plant Cell* **4** , tpc.00804.2018.

Prak, S., Hem, S., Boudet, J., Viennois, G., Sommerer, N., Rossignol, M., Maurel, C. and Santoni, V. (2008). Multiple phosphorylations in the C-terminal tail of plant plasma membrane aquaporins. *Mol. Cell. Proteomics* **7** , 1019–1030.

Qing, D., Yang, Z., Li, M., Wong, W. S., Guo, G., Liu, S., Guo, H. and Li, N. (2016). Quantitative and functional phosphoproteomic analysis reveals that ethylene regulates water transport via the C-Terminal phosphorylation of aquaporin PIP2;1 in *Arabidopsis* .*Mol. Plant* **9** , 158–174.

Qiu, J., Henderson, S. W., Tester, M., Roy, S. J. and Gilliham, M. (2016). SLAH1, a homologue of the slow type anion channel SLAC1, modulates shoot Cl- accumulation and salt tolerance in Arabidopsis thaliana. *J. Exp. Bot.* **67** , 4495–4505.

Roberts, S. K. and Tester, M. (1997). A patch clamp study of Na^+ transport in maize roots. *J. Exp. Bot.***48** , 431–440.

Rodrigues, O., Reshetnyak, G., Grondin, A., Saijo, Y., Leonhardt, N., Maurel, C. and Verdoucq, L. (2017). Aquaporins facilitate hydrogen peroxide entry into guard cells to mediate ABA- and pathogen-triggered stomatal closure. *Proc. Natl. Acad. Sci.***114** , 9200–9205.

Rubio, F., Flores, P., Navarro, J. M. and Martínez, V. (2003). Effects of Ca^{2+}, $K^+$and cGMP on Na+ uptake in pepper plants. *Plant Sci.* **165** , 1043–1049.

Rubio, F., Alemán, F., Nieves-Cordones, M. and Martinez, V.(2010). Studies on Arabidopsis athak5, atakt1 double mutants disclose the range of concentrations at which AtHAK5, AtAKT1 and unknown systems mediate K^+uptake. *Physiol. Plant.* **139** , 220–228.

Takano, J., Wada, M., Ludewig, U., Schaaf, G., Von Wiren, N. and Fujiwara, T. (2006). The Arabidopsis major intrinsic protein NIP5;1 is essential for efficient boron uptake and plant development under boron limitation. *Plant Cell* **18** , 1498–1509.

Tanghe, A., Van Dijck, P., Dumortier, F., Teunissen, A., Hohmann, S. and Thevelein, J. M. (2002). Aquaporin expression correlates with freeze tolerance in baker's yeast, and overexpression improves freeze tolerance in industrial strains. *Appl. Environ. Microbiol.* **68** , 5981–5989.

Tornroth-Horsefield, S., Wang, Y., Hedfalk, K., Johanson, U., Karlsson, M., Tajkhorshid, E., Neutze, R. and Kjellbom, P. (2006). Structural mechanism of plant aquaporin gating. *Nature***439** , 688–694.

Tournaire-Roux, C., Sutka, M., Javot, H. H., Gout, E. E., Gerbeau, P., Luu, D.-T. T., Bligny, R. and Maurel, C. (2002). Cytosolic pH regulates root water transport during anoxic stress through gating of aquaporins. *Nature* **425** , 187–194.

Ueda, M., Tsutsumi, N. and Fujimoto, M. (2016). Salt stress induces internalization of plasma membrane aquaporin into the vacuole in*Arabidopsis thaliana* . *Biochem. Biophys. Res. Commun.***474** , 742–746.

Uehlein, N., Lovisolo, C., Siefritz, F. and Kaldenhoff, R.(2003). The tobacco aquaporin NtAQP1 is a membrane CO_2pore with physiological functions. *Nature* **425** , 734–737.

Van Balkom, B. W. M., Savelkoul, P. J. M., Markovich, D., Hofman, E., Nielsen, S., Van Der Sluijs, P. and Deen, P. M. T. (2002). The role of putative phosphorylation sites in the targeting and shuttling of the aquaporin-2 water channel. *J. Biol. Chem.***277** , 41473–41479.

Van Wilder, V. V. V., Miecielica, U., Degand, H. H. H., Derua, R., Waelkens, E. and Chaumont, F. F. (2008). Maize plasma membrane aquaporins belonging to the PIP1 and PIP2 subgroups are in vivo phosphorylated. *Plant Cell Physiol.* **49** , 1364–1377.

Weaver, C. D., Shomer, N. H., Louis, C. F. and Roberts, D. M.(1994). Nodulin 26, a nodule-specific symbiosome membrane protein from Soybean, is an ion channel. *J. Biol. Chem.* **269** , 17858–17862.

Yaneff, A., Sigaut, L., Gomez, N., Aliaga Fandino, C., Alleva, K., Pietrasanta, L. I. and Amodeo, G. (2016). Loop B serine of a plasma membrane aquaporin type PIP2 but not PIP1 plays a key role in pH sensing. *Biochim. Biophys. Acta - Biomembr.* **1858** , 2778–2787.

Yanochko, G. M. and Yool, A. J. (2002). Regulated cationic channel function in *Xenopus* oocytes expressing *Drosophila*Big Brain. *J. Neurosci.* **22** , 2530–2540.

Yool, A. J., Stamer, W. D. and Regan, J. W. (1996). Forskolin stimulation of water and cation permeability in aquaporin1 water channels. *Science (80-.).* **273** , 1216–1218.

Zelenina, M., Zelenin, S., Bondar, A. A., Brismar, H. and Aperia, A. (2002). Water permeability of aquaporin-4 is decreased by protein kinase C and dopamine. *Am. J. Physiol. Physiol.***283** , F309–F318.

Zhang, W., Zitron, E., Ho, M., Kihm, L., Morath, C., Scherer, D., Hegge, S., Thomas, D., Schmitt, C. P., Zeier, M., et al. (2007). Aquaporin-1 channel function is positively regulated by protein kinase C. *J. Biol. Chem.* **282** , 20933–20940.

Zwiazek, J. J., Xu, H., Tan, X., Navarro-Rodenas, A., Morte, A., Benga, G., Popescu, O., Pop, V. I., Holmes, R., Agre, P., et al.(2017). Significance of oxygen transport through aquaporins. *Sci. Rep.* **7** , 40411.

Figure 1: Exogenous application of membrane permeable cAMP and cGMP analogues as kinase stimulators and the kinase inhibitor H7 influence ionic conductance of *AtPIP2;1* injected oocytes.Oocytes were either untreated or were pre-treated in Low Na^+ Ringers solution that contained 1 mM 8-Br-cAMP (cAMP), 1 mM 8-Br-cGMP (cGMP) or 10 μM H7 dihydrochloride (H7) or H7 followed by cAMP/cGMP. TEVC was performed in a 'Na50' solution. The ionic conductance of treated water injected and *AtPIP2;1* cRNA injected oocytes were normalised to untreated water injected and*AtPIP2;1* cRNA injected oocytes respectively. **(a)**Relative ionic conductance of control oocytes. **(b)** Relative ionic conductance of *AtPIP2;1* injected oocytes. Data was compiled from at least two independent oocytes batches with the exception of the H7 + cNMP treatment where data from one batch of oocytes is represented. Data is represented as mean relative conductance ± SEM where each point represents a single oocyte. Significant differences ($P < 0.001$) are indicated by different letters using one-way ANOVA, Fisher's post test, or by an * (un-paired t-test).

Figure 2: Phosphorylation mimic of AtPIP2;1 S280 and S283 residues influence AtPIP2;1 facilitated cation transport. Oocytes were injected with 46 nL water (Control) or with 46 nL water containing 23 ng*AtPIP2;1* WT (WT) or S280A, S280D, S283A, S283D, A/A, D/A, A/D or D/D cRNA. Representative superimposed currents as a function of time of**(a)** AtPIP2;1 single phosphorylation mutants in 'Na100' (Na^+) and 'K100' (K^+), and**(b)** AtPIP2;1 double phosphorylation mutants in 'Na100' (Na^+). Currents were recorded starting from -40 mV holding potential for 0.5 s and ranging from 40 mV to –120 mV with 20 mV decrements for 0.5 s before following a –40 mV pulse for another 0.5 s. Ionic conductance of oocytes expressing **(c)** AtPIP2;1 single phosphorylation mutants in 'Na100' (Na^+) and 'K100' (K^+), and **(d)** AtPIP2;1 double phosphorylation mutants in 'Na100' (Na^+). Ionic conductance was calculated by taking the slope of a regression of the linear region across the reversal potential (–60 mV to +40 mV). **(e)**Na^+ content of oocytes incubated in 'Na100' for 24 h. Data in (c-e) is compiled from three independent oocyte batches and is shown as mean ± SEM where each data point represents an individual oocyte. Significant differences ($P<0.05$) are indicated by different letters (one-way ANOVA, Fisher's post-test), or by an * (un-paired t-test).

Figure 3.Phosphorylation mimics of AtPIP2;1 S280 and S283 residues influences its osmotic water permeability and the relationship between osmotic water permeability and ionic conductance. Osmotic water permeability (P_{os}) and ionic conductance of water injected (n= 13) and AtPIP2;1 Wild-type (n=37), S280D (n=20) , S280A (n= 13), S283D (n= 19), S283A (n= 17), A/A(n= 25), D/A (n= 16), A/D (n= 27) or AtPIP2;1 D/D (n= 30) cRNA injected oocytes was determined via the swelling assay and TEVC, respectively. **(a)** Ionic conductance collected from multiple batches were allocated into 10 μS bins and the mean ± SEM of each binned group and corresponding P_{os} is plotted. Individual conductance was plotted against the corresponding P_{os} for each oocyte (data shown in Figure S3). A single exponential decay best fit the combined data ($P< 0.005$). The red and blue dashed lines indicate the mean ionic conductance and P_{os} of water injected (control) oocytes. **(b)**Frequency histogram of $P_{os}$for each of the phospho-mimics in decreasing order of the mean P_{os} from left to right. The blue dashed line in each histogram indicated the mean of Pos in water injected (control) oocytes. **(c)** Frequency histogram of ionic conductance for each of the phospho-mimics in increasing order of the mean from left to right. The red dashed line in each histogram indicated the mean of ionic conductance in water injected (control) oocytes.**(d)** Comparison of the order of decreasing $P_{os}$and increasing ionic conductance. Genotypes marked by shaded boxes follow the same relative

order for the change in mean P_{os} and ionic conductance.

Figure 4: Intracellular Na^+ accumulation varied in yeast expressing AtPIP2;1 CTD phosphorylation mimic mutants. Empty vector, AtPIP2;7, AtPIP2;1WT and all versions of CTD of AtPIP2;1 mutants were each expressed in the B31 yeast mutant strain. After suspension in NaCl uptake buffer (70 mM NaCl, 10 mM MES, 10 mM EGTA, pH5.6) for 40 min, intracellular Na^+ contents were measured. Data are compiled from three independent experimental batches each comprised of three independent replicate cultures, and is represented as mean ± SEM. Significant differences ($P<0.05$) are indicated by different letters (one-way ANOVA, Fisher's post-test). N= Empty (10), AtPIP2;7 (7), AtPIP2;1 WT (10), S280A (7), S280D (7), S283A (7), S283D (10), A/D (7), D/A (7), AtPIP2;1 A/A (7) and D/D (7).

Figure 5: Subcellular localisation of AtPIP2;1 wild-type and S280/S283 phospho-mutants in yeast. (a) A control showing that GFP alone results in a diffuse cytosolic localised signal. **(b)** SEC63::RFP endoplasmic reticulum marker. The yeast ER network consists of the prominent nuclear envelope ER domain (nER) and a peripheral or cortical ER domain (cER). The cER lies just beneath the plasma membrane but is not continuous around the perimeter with gaps distinguishing it from plasma membrane localisation (solid triangle). Cytoplasmic tubules link the two ER domains (*). **(c)** Wild-type AtPIP2;1::eGFP localises to a distinct continuous ring of expression around the cell perimeter coinciding with the plasma membrane (PM). GFP signal is also weakly present in the tonoplast of the vacuole (V). In this example, no expression is detected in the nER. **(d-e)** The single phospho-mimetic S280D mutant commonly shows a continuous ring of PM localisation along with a substantially stronger GFP signal co-localised with the ER marker in both the peripheral (open arrow heads) and internal ER networks (nER). **(f)** The single phospho-mimetic S283D mutant shows a clean sharp localisation around the PM with little to no ER co-localisation. Weak GFP signal is occasionally observed in the periphery of the vacuoles (V). **(g-h)** The localisation of the double phosphorylated mimetic D/D mutant occurs almost exclusively in the PM with comparably weak signal detectable in the tonoplast of the vacuole (V) and little to no signal in the ER. **(i)** The double A/D mutant localises to the PM. Approximately half the yeast cells examined also exhibit strong co-localisation to the ER. **(j)** The frequency of yeast cells with GFP signal detected in the PM only versus co-localisation in both the PM and ER. Asterisks (*) denote statistically significant difference (Fisher's exact test p [?] 0.05). N = WtAtPIP2;1(53), S280A(57), S283S(161), S283A(32), S283D(94), A/A(117), D/A(64), A/D(139) , D/D(83).

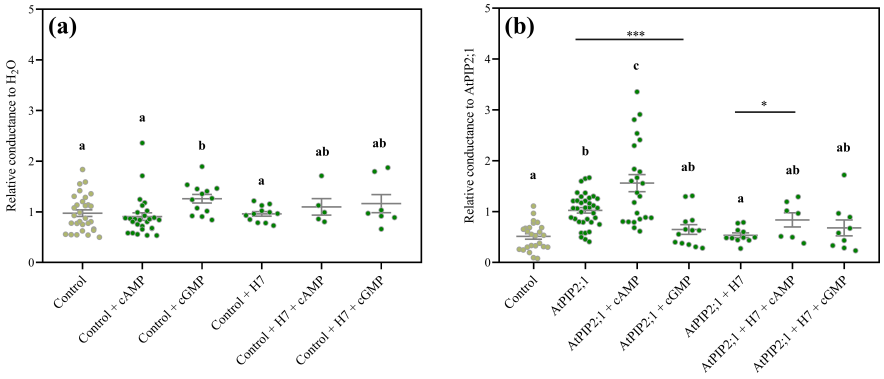

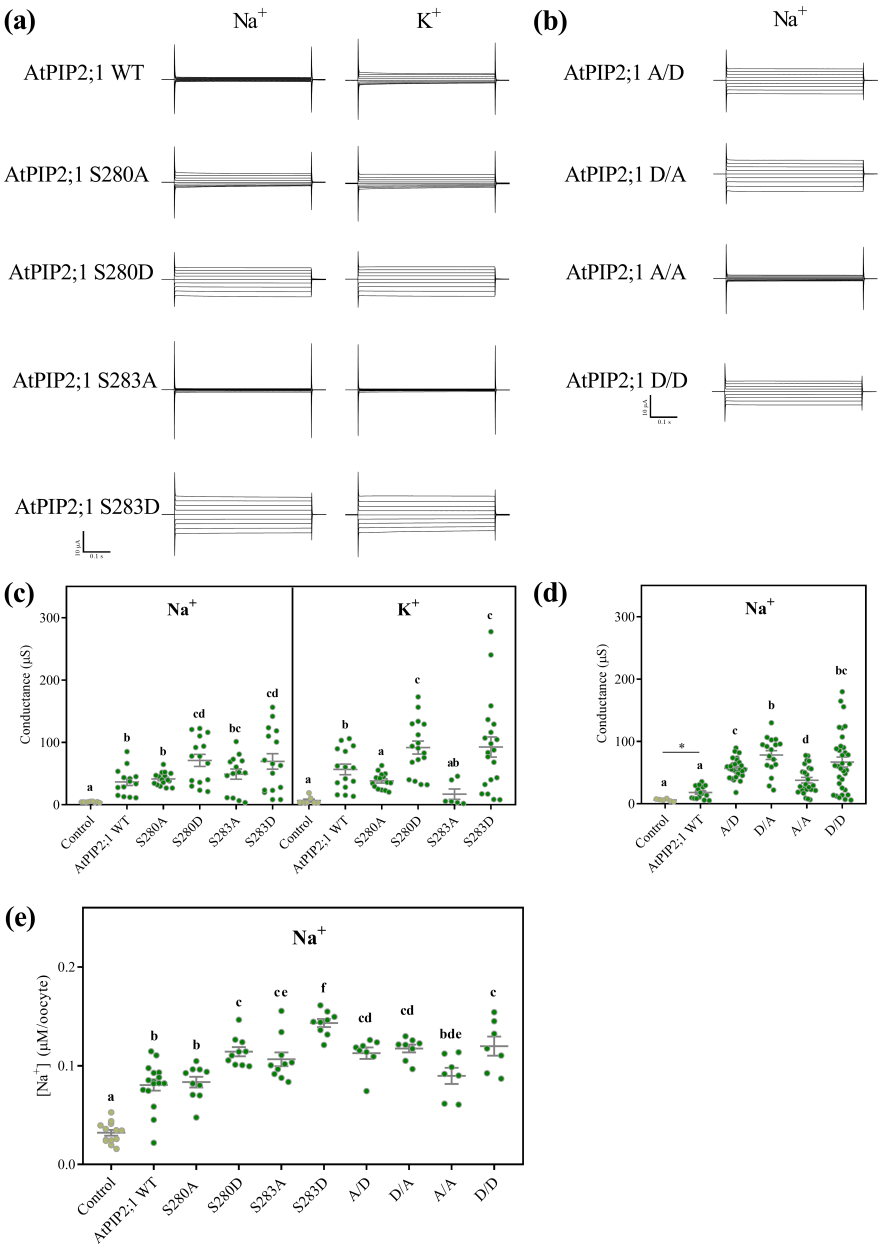

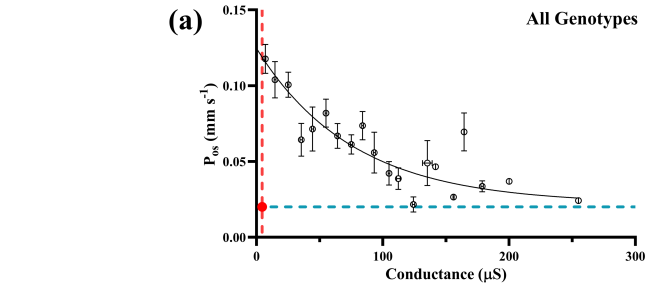

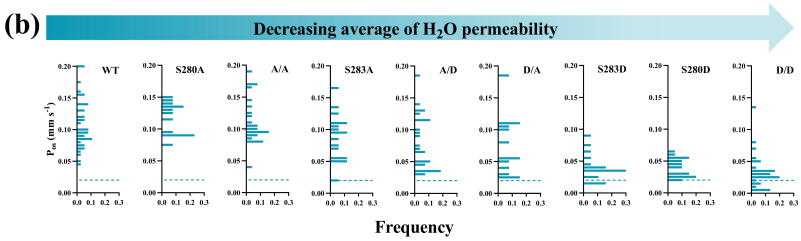

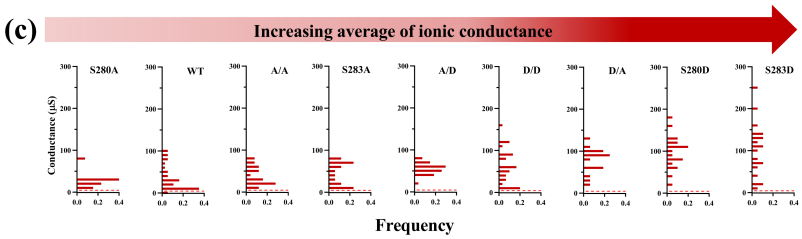

(d)

H_2O permeability (mm s^{-1}) ↓	WT	S280A	A/A	S283A	A/D	D/A	S283D	S280D	D/D
Ionic conductance (µS) ↑	S280A	WT	A/A	S283A	A/D	D/D	D/A	S280D	S283D